Journal of Electroanalytical Chemistry 756 (2015) 77–83

Contents lists available at ScienceDirect

Journal of Electroanalytical Chemistry

journal homepage: www.elsevier.com/locate/jeac

Assembly of magnetic nanoparticles at a liquid/liquid interface. Catalytic effect on ion transfer process

C.I. Cámara [a], L.M.A. Monzón [b,*], J.M.D. Coey [b], L.M. Yudi [a,*]

[a] INFIQC (CONICET-Universidad Nacional de Córdoba). Departamento de Fisicoquímica, Facultad de Ciencias Químicas, Ala 1, Pabellón Argentina, Ciudad Universitaria, 5000 Córdoba, Argentina
[b] School of Physics, SNIAMS Building, Trinity College Dublin, Dublin 2, Ireland

ARTICLE INFO

Article history:
Received 16 February 2015
Received in revised form 4 June 2015
Accepted 30 June 2015
Available online 9 August 2015

Keywords:
Magnetic nanoparticles
Films
Self-assembly
Liquid/liquid interfaces
Electrochemistry

ABSTRACT

The adsorption of cobalt (Co) and cobalt–boron (Co_xB) magnetic nanoparticles (NPs) at a liquid/liquid interface is examined. The Co NPs have a remanent magnetization while the Co_xB is completely demagnetized in the absence of an external magnetic field. Cyclic voltammetry experiments reveal that the adsorption of these NPs at the interface shifts the positive potential limit toward lower values showing that a catalytic effect on the ion transfer process is occurring, while electrochemical impedance spectroscopy demonstrates that their mode of self-assembly is directed by their magnetic properties. Co_xB NPs form a homogeneous film while Co segregates in macroscopic patches, leaving some areas of the interface uncovered.

1. Introduction

The growing interest in ferromagnetic nanoparticles (NPs) is largely motivated to their wide applications in biomedicine [1,2] and biotechnology [3]. They are similar in size to biomolecules [4] and the most common applications in biomedicine are in magnetic resonance imaging [4], drug delivery [5] and hyperthermia cancer therapies [1,6]. Due to their unique properties originating from their small size and large surface area, such as their easy penetration of biomembrane systems, successful strategies to generate biofunctional magnetic nanoparticles for application in protein and pathogen detection have been reported [7].

In the last two decades several kinds of nanoparticle films have been generated at polarized liquid/liquid interfaces. These studies focused on the synthesis, characterization and applications of gold [8,9], platinum [10,11], palladium [11–13], silver [14] and Au–Pd core–shell [9] nanoparticles, demonstrating that the polarization allows us to control the size of the nanoparticles as well as manipulate them [13]. On the other hand, the Langmuir–Schaefer technique has been applied to prepare two-dimensional super paramagnetic films of tridodecylamine-stabilized Co nanoparticles [15]. However, no studies have yet reported the interfacial behavior of magnetic NPs on polarized liquid/liquid interfaces. In the present paper we first characterize the adsorption of Co and Co_xB NPs at these interfaces using cyclic voltammetry (CV) and electrochemical impedance spectroscopy (EIS), complemented with magnetic studies, scanning electron microscopy (SEM), Fourier transform infrared spectroscopy (FT-IR) and energy dispersive X-ray spectroscopy (EDS). The importance of this study is based on the similarity of the water/organic solvent interface with that generated at the cell membrane in the extra-cellular environment [16,17].

2. Materials and methods

CV and EIS were used to characterize the film of NPs at the liquid/liquid interface, using a conventional glass cell (0.94 cm^2 interfacial area) with a four-electrode configuration [17]. Two platinum wires were employed as counter electrodes and the reference electrodes were Ag/AgCl. The reference electrode in contact with the organic solution was immersed in an aqueous solution of 10.0 mM tetraphenylarsonium chloride (TPAsCl, Aldrich). Potential values (E) reported in this work are those which include $\Delta\phi^0_{tr,\ TPAs+} = 0.364$ V for the transfer of the ion $TPAs^+$.

The supporting electrolyte solutions were 10.0 mM $CaCl_2$ (p.a. grade) in ultra-pure water and 10.0 mM tetraphenylarsonium tetrakis (4-chloro phenyl) borate (TPhAsTClPhB) in 1,2-dichloroethane (1,2-DCE, Dorwill p.a.). The pH of the aqueous solution was 5.00. TPhAsTClPhB was prepared by metathesis of tetraphenylarsonium chloride (TPhAsCl, Sigma-Aldrich) and potassium tetrakis (4-chloro phenyl) borate (KTClPhB, Aldrich p.a.).

* Corresponding authors.
E-mail addresses: aranzazl@tcd.ie (L.M.A. Monzón), mjudi@fcq.unc.edu.ar (L.M. Yudi).

http://dx.doi.org/10.1016/j.jelechem.2015.06.020
1572-6657/

The electrochemical cell used was as follows:

Ag	AgCl	TPhAsCl 10.0 mM (w′)	TPhAsTClPhB 10.0 mM (o)	$CaCl_2$ 10.0 mM (pH = 5.00) (w)	AgCl	Ag

Co and Co_xB NPs were prepared according to general protocols [18]. Particularly Co NPs were synthesized employing 9.00 mL of dioctylether (Sigma-Aldrich), 0.50 mL of oleic acid (Sigma-Aldrich) and 0.20 mL of oley amine (Sigma-Aldrich). The mixture was agitated at 80 °C during 1 h, under Ar. Then 0.0470 g $CoCl_2$ was added under constant agitation at T = 150 °C. After dissolution of the salt, 2.00 mL of lithium triethylborohydride ($LiEt_3BH$, Sigma-Aldrich) was injected and temperature was increased to 200 °C during 30 min. Later, the mixture was allowed to stand during 2 h at room temperature and then ethanol was added to precipitate Co NPs, which were separated and washed with acetone.

Co_xB NPs were synthesized dissolving 0.4300 g of $CoCl_2$ and 0.0860 g of sodium butanoate (Sigma-Aldrich) in aqueous/ethanol solution, under stirring at 60 °C. After dissolution, 0.1200 g of $NaBH_4$ was incorporated. The resulting mixture was allowed to stand during 30 min at room temperature. Then Co_xB NPs were magnetically separated from the solution and washed several times.

The NPs dispersion was prepared in ethyl alcohol, at a concentration 0.73 g/mL. It was sonicated for 10 min before use and injected into the 1,2-DCE organic phase, close to the interface. CV and EIS experiments were performed at room temperature 30 min after injection.

CV was performed using a potentiostat with periodic current interruption, for automatic elimination of solution resistance, and a potential sweep generator (LyP Electrónica Argentina). EIS was carried out employing a CHI C700 electrochemical analyzer. The data acquisition and processing were made with a ZPlot/Zview (Scribner Associates Inc.) program. The frequency range was 0.05–4000 Hz, the amplitude of the *ac* perturbation was 10 mV and the constant *dc* potential, *E*, was 0.450 V. Magnetization experiments were performed on a Quantum Desing SQUID 5T magnetometer at room temperature, FT-IR spectra were recorded on a Bruker IFS28 spectrophotometer, SEM images were taken on a Zeiss Auriga microscopy and EDS measurement were made on a Carl Zeiss microscope FE-SEM Σigma. A PANalytical X'pert Pro X-ray diffractometry (XRD) system with a Cu Kα (λ = 1514.1 pm) X-ray source and an X'celerator IP detector was used to characterize the crystal structure of the nanoparticles.

3. Result and discussion

3.1. General characterization of MNPs

The characterization of MNPs was carried out employing different techniques for different purposes: magnetization curves were obtained for the evaluation of the magnetic properties of Co and C_xB NPs, XRD experiments were performed to analyze the crystal structure of both MNPs, while EDS and FT-IR experiments allowed the characterization of the NPs composition including the surfactants adsorbed on the NPs' surface.

Fig. 1 shows the magnetizations loops for Co and Co_xB NPs as a function of the applied magnetic field. The saturation magnetizations (M_s) were 45 $A \cdot m^2 \cdot kg^{-1}$ and 30 $A \cdot m^2 \cdot kg^{-1}$ for Co and Co_xB, respectively. The main difference between the samples is their coercivity, $\mu_0 H_0$ = 25 mT for Co NPs and 2 mT for Co_xB (see Fig. 1, inset), which means that the Co NPs are still magnetized when the external magnetic field is switched off, while the Co_xB NPs are not (Co NPs remaining value, M_r, is 28% of M_s). The saturation magnetization of both samples is reduced from its bulk value mainly by the oxidization of the surface and due to the B and C contents.

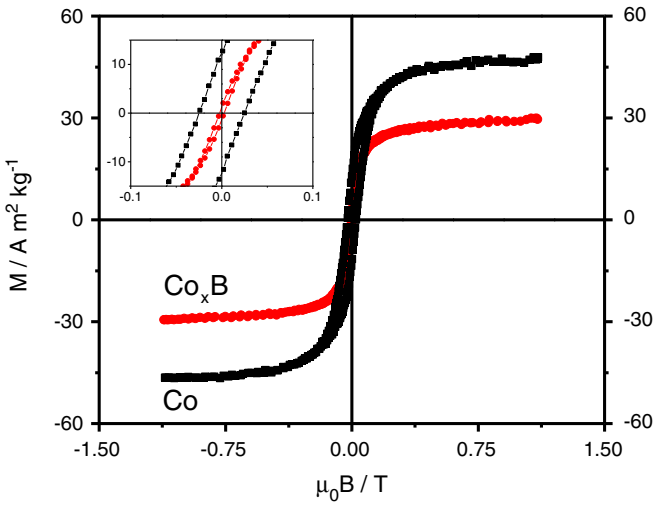

Fig. 1. Magnetic hysteresis loops for Co and Co_xB NPs. The inset shows a magnification near zero-field.

Fig. 2 shows XRD patterns of both types of magnetic nanoparticles. The data in red corresponds to Co_xB and the one shown in black to Co. There are clear differences in their crystal structures for these two types of samples: the pattern of Co_xB is typical of amorphous solids as there are no reflections that can be clearly distinguished whereas Co presents several reflections arising from the (100), (002), (101), (102), (110) and (112) planes of its hexagonal structure. For randomly oriented hcp Co powders, the intensity of the 101 reflection is much stronger than the intensity of the (002) or (100), whereas here the XRD pattern of Co nanopowder shows that the peak corresponding to the (002) reflection has a much stronger intensity than the rest. This indicates that the Co nanoparticles have a preferential orientation along the c-axis driven by the magnetocrystalline anisotropy of hcp Co. The observed room temperature coercivity of these samples suggests the existence of hcp cobalt.

Co NPs exhibit an elongated structure with an average crystal size of 25 nm (standard deviations σ = 12%) while the average size of amorphous Co_xB NPs is 30 nm (standard deviations σ = 15%). Given the non-zero magnetization of Co NPs, during the synthesis, they tend to

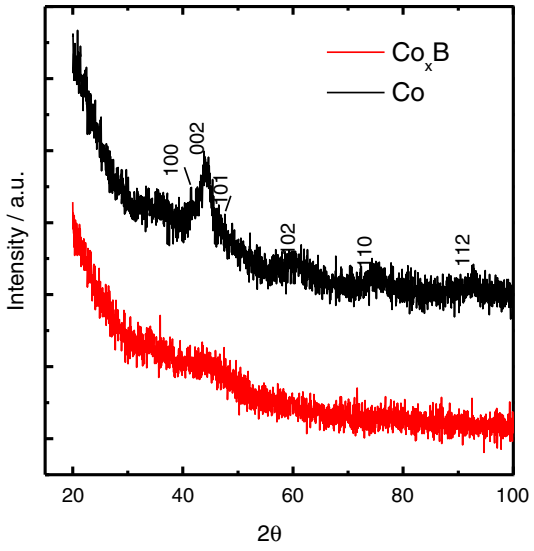

Fig. 2. XRD patterns for Co (▬) and Co_xB (▬) NPs.

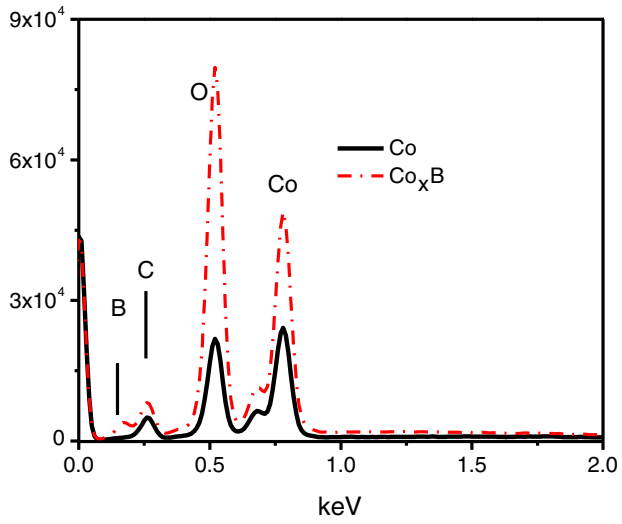

Fig. 3. EDS spectra for Co (▬) and Co_xB (—●—) NPs.

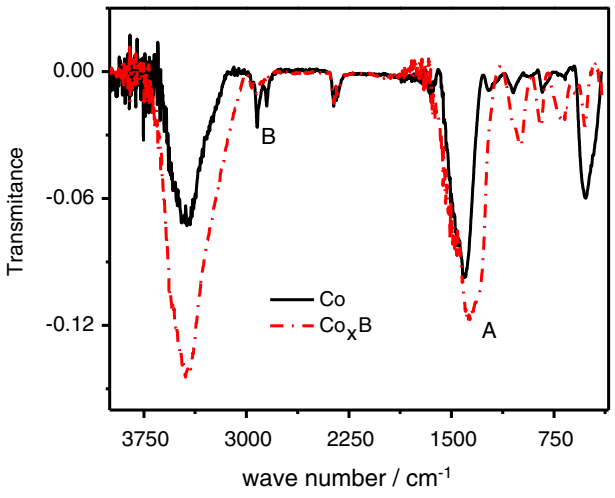

Fig. 4. FT-IR spectra for Co (▬) and Co_xB (—●—) NPs.

align their magnetic dipoles along a longitudinal direction, giving rise to the needle or rod-like shapes as also evidenced by XRD [19].

EDS and FT-IR experiments were performed to characterize the surfactants adsorbed on the NPs' surface. Fig. 3 shows EDS spectra obtained for Co and Co_xB NPs. Both samples contain cobalt (Co), carbon (C) and oxygen (O). Furthermore, the EDS spectrum of Co_xB also shows the presence of small amount (less than 3.0%) of boron (B). From these EDS spectra, the relative percentage of each element present in both samples was determined and summarized in Table 1. As can be observed, significant percentages of C and O are present in both samples, indicating the presence of hydrocarbon chains with functional groups containing O at NP's surfaces. Taking into account that oleic acid and butanoic acid were added, as stabilizing agents, during the synthesis of Co and Co_xB Nps, respectively, it can be concluded that these NPs are derivatized with the respective acids at their surfaces. The exact composition of these particles is still a subject under debate given that the reaction mechanism for the reduction of Co^{2+} ions by BH_4^- is not known [20]. U. B. Demirci et al. have surveyed the literature and postulate that the particles have a core–shell structure, with a core composition consisting of nanosized Co^0, cobalt boron alloys (Co–B) and cobalt borides (Co_xB, with x from 1 to 3). Nevertheless, as stated by these authors, the determination of x is neither simple nor reliable due to the small weight of B and to the fact that some of the B content accounts for borate bridges that result from partial hydrolysis of BH_4^- during the synthesis.

The FT-IR spectra were obtained from solid samples incorporated in KBr pellet at a concentration 0.40% w/w (Fig. 4). Sharp peaks between 1300–1500 cm^{-1} (A) can be clearly noted, which can be attributed to carboxylic groups attached to Co, or to the signal of carbonyl groups in the acid, shifted toward lower wave numbers with respect to the signal of the carboxylic acid in solution [21]. The absence of a broad band between 3500 and 3100 cm^{-1} indicates that the O–H stretching is not present. Other important peaks are found in the region between 3000–2700 cm^{-1} (B), which correspond to the stretching of C–H bond on methyl groups in the hydrocarbon tails [22]. The lower intensity of these peaks for Co_xB sample could be attributed to the lower amounts of methyl groups present in the organic chain. Based on these results, the presence of deprotonated carboxylic groups, and therefore of negative charge, on both types of particles is confirmed. It is a known fact that these groups bind to the surface of the metal. However, they contribute to the surface charge of the particle and make it hydrophilic. Indeed, NPs do not exhibit surface pressure–molecular area isotherms when they are injected into the surface of an aqueous subphase in a Langmuir balance (data not shown). Rather, they are directed to the aqueous subphase. A reasonable explanation for this behavior is based on the formation of a bilayer in the surface of the NPs, with a first layer in which the carboxyl groups bind to Co and the hydrophobic chains are oriented outward, while the second layer is bonded to the first one, through the hydrophobic chains, leaving the carboxyl groups exposed to the surface.

Table 1
Relative percentage for each element present in Co and Co_xB NPs.

Element	Relative percentage Co	Relative percentage Co_xB
Co	75.9	70.1
O	15.4	24.1
C	8.1	5.1
B	–	<3.0

3.2. Electrochemical characterization at the liquid/liquid interface

Fig. 5a shows the voltammetric response recorded before and after the injection of the Co dispersions. The increase of the NPs' concentration at the interface narrows the potential window from the positive end, which is determined by the Ca^{2+} transfer from the aqueous to the organic phase. Similar behavior was obtained with Co_xB. These observations are summarized in Fig. 5b, where the potential shift with respect to the bare interface (ΔE/V), measured at $I = 14$ μA, is shown as a function of the volume of colloidal solution injected. N. Younan et al. [8] reported similar effect upon the injection of methanol, which induced higher transfer currents on the extremities of the potential window, particularly at positive potential values. Therefore, in the present case, the results obtained upon addition of pure ethanol are also included in Fig. 5b for comparison. Data shown in this figure are the mean values calculated from five experimental points and error bars correspond to dispersion analysis of these points. The potential shift observed is enhanced in the presence of the NPs, indicating that they alter the properties of the liquid/liquid interface more than pure ethanol. The presence of ethanol generates a more diffuse aqueous/1,2-DCE interface as it increases the local permittivity. Under this condition, the Gibbs energy of Ca^{2+} transfer is lower than in the absence of ethanol, which is revealed as a shift in the positive potential limit [8]. Nevertheless, this effect is even higher in the presence of NPs because the particle charge modifies the surface potential. This result was confirmed by doubling the concentration of NPs' solutions, and thus the volume injected was one half of that used in the experiments in Fig. 5, resulting in the same

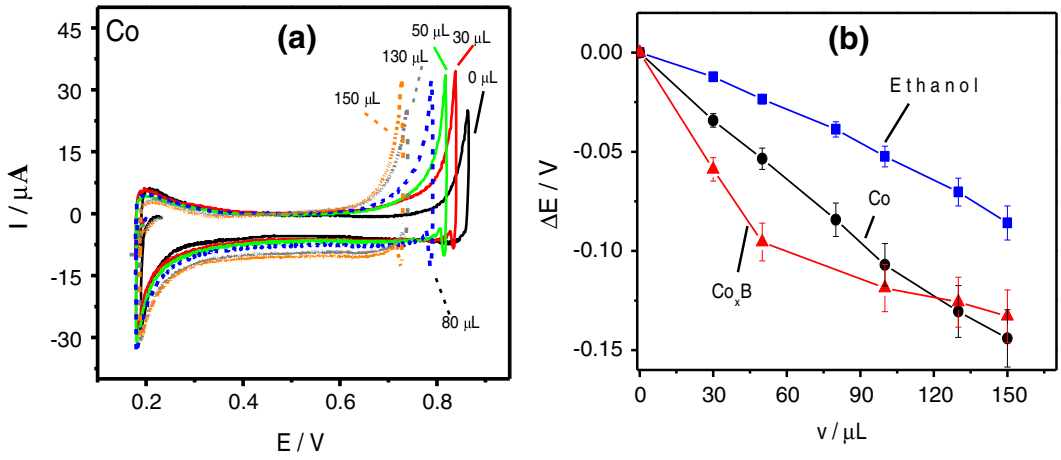

Fig. 5. (a) Cyclic voltammograms obtained at $v = 0.050\ Vs^{-1}$ after the injection of different volumes of Co NPs dispersed in ethanol. (b) Transfer potential shift measured at $I = 14\ \mu A$, as a function of the amount injected of pure ethanol (■), Co (●) and Co_xB (▲).

shifts of potential limit for the same amount of NPs injected (data not shown). It is also worth noting that a similar effect was observed with other aqueous electrolytes containing di or trivalent cations ($CoCl_2$, $DyCl_3$, data not shown).

Similar catalytic activity was also reported by Y. Gründer et al. [9] for Au and Au–Pd core–shell nanoparticles at the liquid–liquid interface, in the presence of 1,1′-dimethylferrocene in the organic phase, used as reducing agent. They demonstrated that these particles catalyze interfacial oxygen reduction, and established the correlations between the catalytic activity and particle radius, surface area and concentration.

J.A. Manzanares et al. [23] studied, experimentally and theoretically, the transfer of cations across a zwitterionic phospholipid monolayers at a liquid/liquid interface. They reported evidences for the enhanced rate for cation transfer due to the presence of the monolayer which changes the charge distribution in the double layer. In this way, they carried out a theoretical description based on the electrical double layer correction to the Butler–Volmer equation, coupled to a solution of the Poisson–Boltzmann equation across the interfacial region, obtaining the following expression for the flux density, j_i, corresponding to the transfer of the ion i:

$$j_i = k^0_{i,app}\left[c_i^{w*} e^{\alpha z_i f\left(\Delta^w_o\phi - \Delta^w_o\phi^0_i\right)} - c_i^{o*} e^{(\alpha-1) z_i f\left(\Delta^w_o\phi - \Delta^w_o\phi^0_i\right)}\right] \quad [1]$$

where $c_i^{w\,*}$ and $c_i^{o\,*}$ are the ion i concentration at the bulk of aqueous and organic phase respectively, z_i is the ion charge, $f = F/RT$, $\Delta^w_o\phi$ is the potential difference across the liquid/liquid interface, $\Delta^w_o\phi^0_i$ is the standard transfer potential of the ion i and $k^0_{i,app}$ is an apparent standard rate constant equal to:

$$k^0_{i,app} = k^0_i e^{(1-\alpha) z_i f\left(\phi^w - \phi^w_{OHP}\right)} . e^{-\alpha z_i f\left(\phi^o_{OHP} - \phi^o\right)} \quad [2]$$

where ϕ^w and ϕ^0 are the electrical potentials at the positions x^w_0 and x^o_0 just outside the diffuse electrical double layer at the aqueous and organic side of the interface, respectively and ϕ^w_{OHP} and ϕ^o_{OHP} are the electrical potentials at the outer Helmholtz planes. In this way, $k^0_{i,app}$ depends on the potential distribution. Assuming a sharp interface model and neglecting the finite size of the transferring ion, $x^w_{OHP} = x^o_{OHP} = 0$ and $\phi^w_{OHP} = \phi^o_{OHP} = \phi(0)$, so that $\Delta^w_o\phi_{OHP} = 0$. Thus, for $\alpha \approx 1/2$, the following relationship between the apparent rate constant and the electrical potential at the liquid/liquid interface, $\phi(0)$, was deduced by the authors as [23]:

$$k^0_{i,app} = k^0_i e^{-z_i f\tilde{\phi}(0)} \quad [3]$$

where $\tilde{\phi}(0)\phi(0) - (\phi^w - \phi^o)/2$ represents the potential at the interface measured with respect to the average potential of the aqueous and the organic phase. In this way, J.A. Manzanares et al. postulated that the presence of zwitterionic phospholipids at the interface can affect the ion transfer rate altering the electric potential $\tilde{\phi}(0)$, due to the charge present in the polar head groups, or the standard rate constant, k^0_i. In the present study, the adsorption of charged NPs at the interface probably produces the first effect leading to changes in $\tilde{\phi}(0)$ and thus enhancing the ion transfer rate. J.A. Manzanares et al. defined the enhancement factor as the ratio of apparent rate constant in the presence and in the absence of phospholipids [23]:

$$\frac{k^0_{i,app}(\text{presence})}{k^0_{i,app}(\text{absence})} = e^{-z_i f\left[\tilde{\phi}(0)_{\text{presence}} - \tilde{\phi}(0)_{\text{absence}}\right]} \quad [4]$$

and analyzed the effect of polar head group size, ion concentration and Galvani potential on this ratio.

In the present paper we calculated this enhancement factor as the ratio $I_{\text{with NPs}}/I_{\text{without Nps}}$ ($I_{\text{without Nps}}$ corresponds to current values in absence of NPs but in presence of equivalent volumes of pure ethanol). Fig. 6a and b show the variation of the resulting enhancement ratio as a function of the applied potential for increasing amounts of Co and Co_xB NPs respectively. As can be observed an enhancement effect is evident for both NPs, mainly at low potentials values. This activation effect increases with potential, probably due to an improvement in the adsorption process favored at potential values higher than the zero charge potential, or to specific interaction between Ca^{2+} ions and carboxylic groups present at NPs surface, improved by interfacial accumulation of Ca^{2+} at high potentials values. This increase in activation factor occurs up to a value equal to $E = 0.720$ V or $E = 0.800$ V for Co or Co_xB NPs, from which the enhancement factor begins to decline in agreement with the theoretical predictions of J.A. Manzanares et el. [23]. This decrease in the enhancement factor can be interpreted considering the space charge distribution [23]: the increasing applied potential difference involves an increasing charge separation, when this charge separation is lower than the charge density brought by the NPs, large perturbations of the electric potential distribution are expected in the presence of NPs, on the contrary, the contribution of these perturbations is less important at higher charge separations, i.e. higher applied potentials.

The enhancement effect described above, have to be related to the specific interaction of divalent cations, Ca^{2+}, with carboxylic groups [24]. To verify this hypothesis, cyclic voltammetry experiments were performed in the presence of a referent cation as tetraethylammonium,

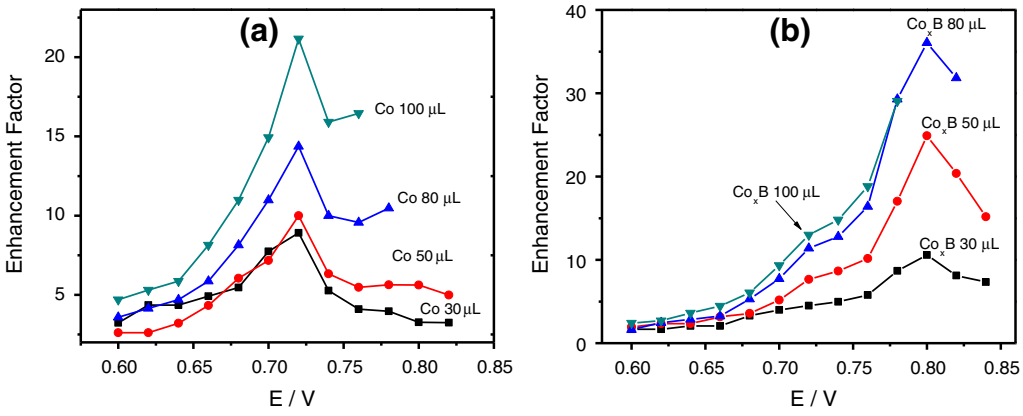

Fig. 6. Enhancement factor as function of applied potential for (a) Co and (b) Co_xB NPs, calculated for voltammograms at Fig. 5.

TEA^+. The results are shown in Fig. 7. As it can be noticed TEA^+ transfer is not affected by the Co or Co_xB NPs films. These results allow us to arrive to two important conclusions: the monolayer does not produce any blocking effect and the electrocatalytic effect of nanoparticles is not only due to the electrical double layer correction but also to a specific interaction of divalent cations with carboxylic groups.

Fig. 8a shows Bode plots obtained in the absence and presence of 80 µL of Co or Co_xB dispersions at $E = 0.450$ V. The EIS response obtained for the bare interface could be fitted using the Randles circuit shown in Fig. 8b, where R_s is the solution resistance, CPE_{dc} is a constant phase element which takes into account the double layer capacity and R_{tc} is the charge transfer resistance. When Co_xB NPs were present at the interface, the results were also fitted with the Randles circuit, indicating that there is an homogeneous assembly of NPs at the interface [25]. Under this condition R_{tc} and CPE_{tc} represent the charge transfer resistance and the double layer capacity in the presence of NPs and the results obtained differ significantly from those obtained in absence of NPs, with a marked increase in capacity with the volume of colloidal solution injected from C = 25 µF, corresponding to bare interface, obtained in absence of NPs, to C = 120 µF, after adding 150 µL of NPs suspension. If Co NPs are present at the interface, the EIS response could no longer be fitted with a Randles model. Instead, the results fit better with the equivalent circuit shown in Fig. 8c, which can be interpreted by considering the formation of an inhomogeneous film, in which different domains are present, with uncovered (bare, without NPs) zones characterized by a charge transfer resistance (R_4), a double-layer capacity (C_1) and a solution resistance within the pores (R_3); and another domains corresponding to covered zones (domains with NPs) and characterized by a double-layer capacity (CPE_1) and a charge transfer resistance through the NPs layer (R_2). In this case, the capacity corresponding to the covered domains also increases from C = 25 µF (bare interface) to C = 50 µF, after the injection of 150 µL of NPs suspension, while the capacity of bare domains slightly decreases with the volume of colloidal solution injected. The differences found in the interfacial behavior between the Co and Co_xB NPs, are due not only to their small differences in morphology but also to the tendency of Co NPs to clump together [26,27]. These findings from the EIS experiments are consistent with the macroscopic observation at liquid/liquid interfaces of large area, in which different domains for Co NPs or a more homogeneous film for Co_xB NPs are clearly distinguished after the injection of a large volume of NPs suspension (600 µL). Co nanoparticles adsorbed at the interface form a film of macroscopic clusters which can be directly observed with a video camera. Images have been processed employing the software "imagej". The diameter mean value obtained for these domains of Co nanoparticles in the sampled region of the interface was 0.147 mm.

Fig. 9 shows the variation of interfacial C for Co and Co_xB NPs as a function of the volume of Nps colloidal solution injected at the liquid/liquid interface. C values were obtained from the fitting of EIS recorded at $E = 0.450$ V for each volume of NPs injected at the interface, employing the equivalent circuits described above. As it was mentioned, EIS experiments for Co_xB NPs were fitted with the Randles circuit leading to the conclusion that a homogeneous layer of NPs is present at the interface. Therefore, a unique C value was obtained from the fitting,

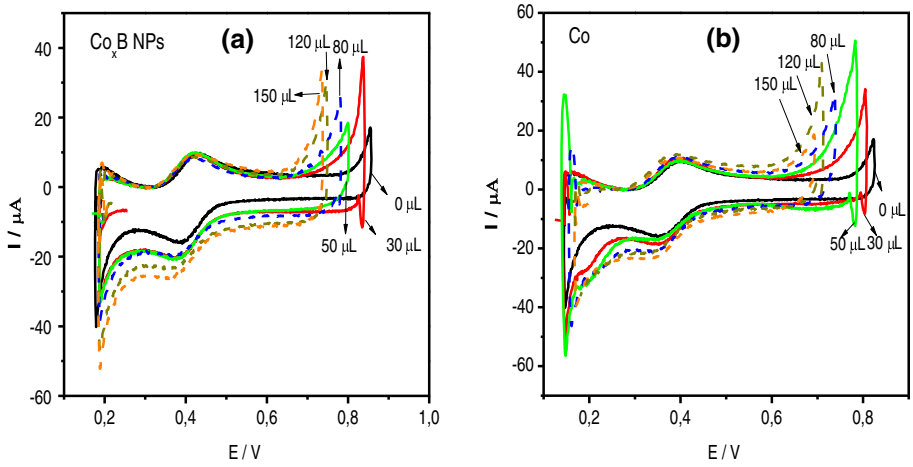

Fig. 7. Cyclic voltammograms for TEA^+ transfer process in the absence (▬) and presence of different volumes of Co_xB (a) and Co NPs (b). Concentration of TEA^+ in aqueous phase = 5.0×10^{-4} M. $v = 0.050$ V s^{-1}.

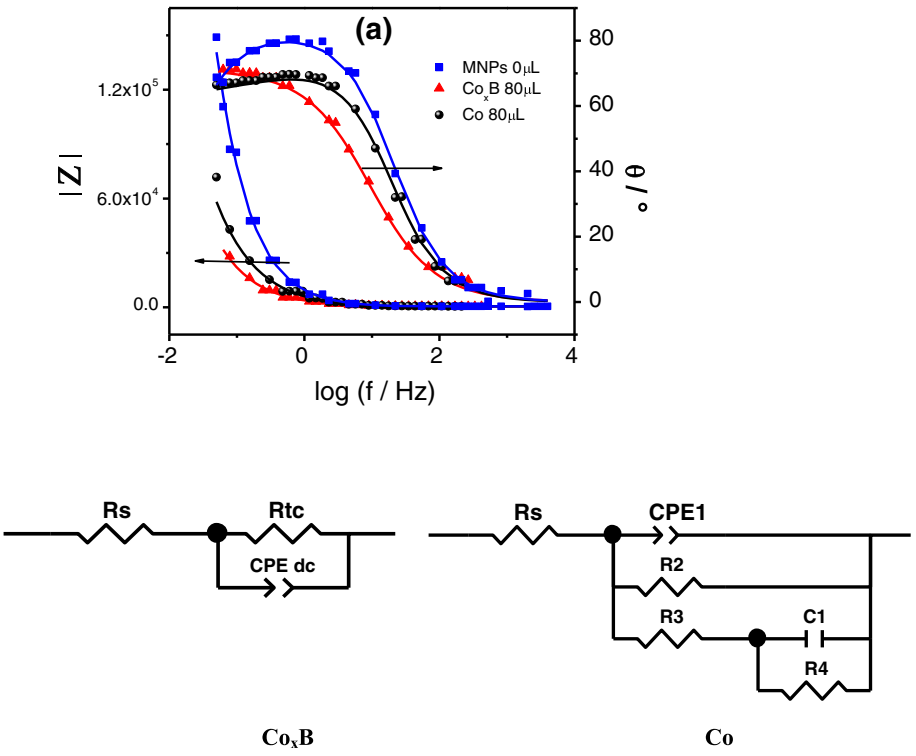

Fig. 8. (a) Experimental Bode plots in the absence (■) or in presence of (●) Co or (▲) Co$_x$B NPs. (b) and (d) are the equivalent circuits employed to fit EIS results and the corresponding photographs obtained for the NPs interfacial films at a large liquid/liquid interface.

which correspond to the monolayer capacity value. As can be observed in the Fig. 8, a continuous increase of C can be observed. In the case of Co Nps, the presence of different domains was postulated from the fitting of EIS experiments, so that, two C values can be distinguished at each volume added, corresponding to covered and uncovered zones. In the first case C values continuously increase, in similarly to the effect produced by Co$_x$B NPs, and in the second case, uncovered domains, C decreases due to the increase of covered domains as the amount of injected Nps increases.

N. Younan et al. [8] explained the enhancement of the interfacial capacity produced by an adsorbed monolayer of citrate-coated gold nanoparticles taking into account the increase of the interfacial charge density or the increase in the interface roughness, which influences the interfacial capacity. In the present system, the last effect should be less significant, given that no marked increase in currents is observed in the whole voltammetric response (Fig. 5a).

Taking the potential shift ΔE as −0.130 V (Fig. 5b) and the difference in capacity values of bare and Co$_x$B-coated interface as 95 μF, and considering that $\Delta C = q / \Delta E$, the charge brought onto the interface by the nanoparticles, q, can be calculated as 7.7×10^{13} e$^-$. Considering the NPs diameter is 30 nm, the NPs area can be estimated as 7.07×10^{-12} cm^2. If the film is a monolayer of NPs, and the interfacial area is 0.94 cm^2, the total number of NPs at the interface should be 1.33×10^{11}. This would mean that each particle has an effective charge of 580 e$^-$. Therefore, it seems most likely that the arrangement of Co$_x$B NPs at the interface has a multilayered structure.

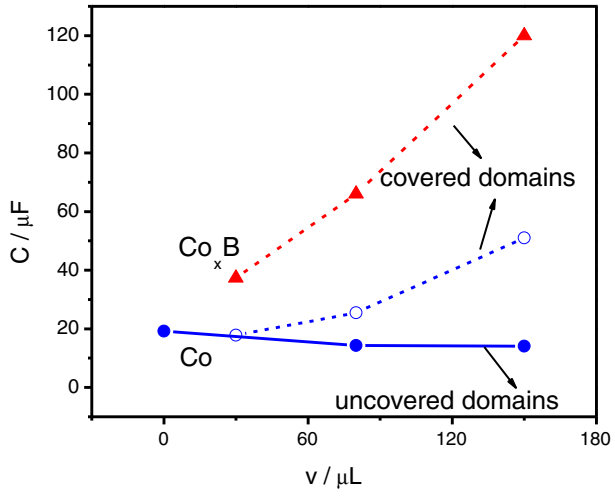

Fig. 9. Capacity (C) as function of injected volume (V) of colloidal solution of Nps at the liquid/liquid interface.

4. Conclusions

This is the first study of the adsorption of magnetic nanoparticles at an electrified liquid/liquid interface. The surface derivatization with carboxylic groups, which provides negative charge to the interface, lead to a modification of the interfacial potential, producing a catalytic effect on Ca^{2+} transfer from the aqueous to the organic phase, evidenced by a shift of transfer potential toward lower values. They also enhance the interfacial capacitance, which we correlate with the presence of surface charge on these particles, given by the carboxylic groups of the surfactants.

The self-assembly of ferromagnetic NPs at liquid/liquid interfaces is influenced by inter particle magnetic dipole interactions. The Co$_x$B NPs spread out over the interface to uniform films because they are not magnetized. On the other hand, Co NPs segregate into separate domains, as the attractive forces established among them are stronger than their tendency to spread at an interface. A way to control the remanence magnetization of the Co NPs and therefore their interfacial self-assembly, would be to synthesize particles with different particle size around the critical single-domain size [27,28].

Acknowledgments

Financial support from CONICET (PIP 112-201101-00011), FONCyT (PICT-Raices grant 2013-0822), SECyT-UNC and 13/ERC/12561 are gratefully acknowledged. The authors thank to Dr. Maximiliano Burgos for his contribution in FT-IR experiments.

References

[1] C.S.S.R. Kumar, F. Mohammad, Magnetic nanomaterials for hyperthermia-based therapy and controlled drug delivery, Adv. Drug Deliv. Rev. 63 (2011) 789–808.
[2] J. Rivas, M. Bañobre-López, Y. Piñeiro-Redondo, B. Rivas, M.A. López-Quintela, Magnetic nanoparticles for application in cancer therapy, J. Magn. Magn. Mater. 324 (2012) 3499–3502.
[3] T. Moore, H. Chen, R. Morrison, F. Wang, J.N. Anker, F. Alexis, Nanotechnologies for noninvasive measurement of drug release, Mol. Pharm. 11 (2014) 24–39.
[4] X.L. Liu, H.M. Fan, Innovative magnetic nanoparticle platform for magnetic resonance imaging and magnetic fluid hyperthermia applications, Curr. Opin. Chem. Eng. 4 (2014) 38–46.
[5] L. Philosof-Mazor, G.R. Dakwar, M. Popov, S. Kolusheva, A. Shames, C. Linder, S. Greenberg, E. Heldman, D. Stepensky, R. Jelinek, Bolaamphiphilic vesicles encapsulating iron oxide nanoparticles: new vehicles for magnetically targeted drug delivery, Int. J. Pharm. 450 (2013) 241–249.
[6] S. Nazir, T. Hussain, A. Ayub, U. Rashid, A.J. MacRobert, Nanomaterials in combating cancer: therapeutic applications and developments, Nanomed. Nanotechnol. Biol. Med. 10 (2014) 19–34.
[7] H. Gu, K. Xu, C. Xu, B. Xu, Biofunctional magnetic nanoparticles for protein separation and pathogen detection, Chem. Commun. 9 (2006) 941–949.
[8] N. Younan, M. Hojeij, L. Ribeaucourt, H.H. Girault, Electrochemical properties of gold nanoparticles assembly at polarised liquid|liquid interfaces, Electrochem. Commun. 12 (2010) 912–915.
[9] Y. Gründer, M.D. Fabian, S.G. Booth, D. Plana, D.J. Fermín, P.I. Hill, R.A.W. Dryfe, Solids at the liquid–liquid interface: electrocatalysis with pre-formed nanoparticles, Electrochim. Acta 110 (2013) 809–815.
[10] A. Trojánek, J. Langmaier, Z. Samec, Random nucleation and growth of Pt nanoparticles at the polarised interface between two immiscible electrolyte solutions, J. Electroanal. Chem. 599 (2007) 160–166.
[11] M. Platt, R.A.W. Dryfe, Structural and electrochemical characterisation of Pt and Pd nanoparticles electrodeposited at the liquid/liquid interface: part 2, Phys. Chem. Chem. Phys. 7 (2005) 1807–1814.
[12] C. Johans, K. Kontturi, D.J. Schiffrin, Nucleation at liquid|liquid interfaces: galvanostatic study, J. Electroanal. Chem. 526 (2002) 29–35.
[13] R.M. Lahtinen, D.J. Fermín, H. Jensen, K. Kontturi, H.H. Girault, Two-phase photocatalysis mediated by electrochemically generated Pd nanoparticles, Electrochem. Commun. 2 (2000) 230–234.
[14] C. Johans, J. Clohessy, S. Fantini, K. Kontturi, V.J. Cunnane, Electrosynthesis of polyphenylpyrrole coated silver particles at a liquid–liquid interface, Electrochem. Commun. 4 (2002) 227–230.
[15] E. Pohjalainen, M. Pohjakallio, C. Johans, K.S. Kontturi, J.V.I. Timonen, O. Ikkala, R.H.A. Ras, T. Viitala, M.T. Heino, E.T. Seppälä, Cobalt nanoparticle Langmuir–Schaefer films on ethylene glycol subphase, Langmuir 26 (2010) 13937–13943.
[16] C.I. Cámara, M.V.C. Quiroga, N. Wilke, A. Jimenez-Kairuz, L.M. Yudi, Effect of chitosan on distearoylphosphatidylglycerol films at air/water and liquid/liquid interfaces, Electrochim. Acta 94 (2013) 124–133.
[17] C.I. Cámara, L.M. Yudi, Potential-mediated interaction between dextran sulfate and negatively charged phospholipids films at air/water and liquid/liquid interfaces, Electrochim. Acta 113 (2013) 644–652.
[18] T. Hyeon, Chemical synthesis of magnetic nanoparticles, Chem. Commun. 8 (2003) 927–934.
[19] Y. Min, M. Akbulut, K. Kristiansen, Y. Golan, J. Israelachvili, The role of interparticle and external forces in nanoparticle assembly, Nat. Mater. 7 (2008) 527–538.
[20] U.B. Demirci, P. Miele, Cobalt in $NaBH_4$ hydrolysis, Phys. Chem. Chem. Phys. 12 (2010) 14651–14665.
[21] K. Simeonidis, S. Mourdikoudis, A. Vilalta-Clemente, I. Tsiaoussis, M. Angelakeris, O. Kalogirou, Shape and composition oriented synthesis of cobalt nanoparticles, Physics of Advanced Materials Winter School2008.
[22] Z. Fereshteh, M. Salavati-Niasari, K. Saberyan, S.M. Hosseinpour-Mashkani, F. Tavakoli, Synthesis of nickel oxide nanoparticles from thermal decomposition of a new precursor, J. Clust. Sci. 23 (2012) 577–583.
[23] J.A. Manzanares, R.M. Allen, K. Kontturi, Enhanced ion transfer rate due to the presence of zwitterionic phospholipid monolayers at the ITIES, J. Electroanal. Chem. 483 (2000) 188–196.
[24] T. Bala, B.L. Prasad, M. Sastry, M.U. Kahaly, U.V. Waghmare, Interaction of different metal ions with carboxykic acid group: a quantitative study, J. Phys. Chem. A 111 (2007) 6183–6190.
[25] L.M.A. Monzón, L.M. Yudi, Electrochemical study of flunitrazepam partitioning into zwitterionic phospholipid monolayers, Electrochim. Acta 51 (2006) 1932–1940.
[26] L.M.A. Monzon, K. O'Neill, Y. Sheth, M. Venkatesan, J.M.D. Coey, Fabrication of multisegmented magnetic wires with micron-length copper spacers, Electrochem. Commun. 36 (2013) 96–98.
[27] J.M.D. Coey, Magnetism and Magnetic Materials, Cambridge University Press, New York, 2010.
[28] L.M.A. Monzon, K. Ackland, S. Mosivand, M. Venkatesan, J.M.D. Coey, The role of polyaniline in the formation of iron-containing nanocomposites, J. Nanopart. Res. 15 (2013).